Lawrence Berkeley National Laboratory
LBL Publications

Title
In-situ characterization of highly reversible phase transformation by synchrotron X-ray Laue microdiffraction

Permalink
https://escholarship.org/uc/item/6r33b3fj

Journal
Applied Physics Letters, 108(21)

ISSN
0003-6951

Authors
Chen, Xian
Tamura, Nobumichi
MacDowell, Alastair
et al.

Publication Date
2016-05-23

DOI
10.1063/1.4951001

Peer reviewed

eScholarship.org Powered by the California Digital Library
University of California

In-situ characterization of highly reversible phase transformation by synchrotron X-ray Laue microdiffraction

Xian Chen,[1,2] Nobumichi Tamura,[2] Alastair MacDowell,[2] and Richard D. James[3]
[1)] *Hong Kong University of Science and Technology, Clear Water Bay, Hong Kong*
[2)] *Advanced Light Source, Lawrence Berkeley National Lab, Berkeley, CA 94720 USA*
[3)] *University of Minnesota, Minneapolis, MN 55455 USA*

(Dated: 5 February 2016)

The alloy $Cu_{25}Au_{30}Zn_{45}$ undergoes a big first-order phase transformation (6% strain) and shows high reversibility under thermal cycling and unusual martensitc microstructure in sharp contrast to its nearby compositions. This alloy was discovered by systematically tuning composition so its lattice parameters satisfy the Cofactor Conditions (i.e., the kinematic conditions of compatibility between phases). It was conjectured that satisfaction of these conditions is responsible for the enhanced reversibility as well as the observed unusual fluid-like microstructure during transformation, but so far there has been no direct evidence confirming that these observed microstructures are those predicted by the Cofactor Conditions. To verify this hypothesis, we use synchrotron X-ray Laue microdiffraction to measure the orientations and structural parameters of variants and phases near the austenite/martensite interface. Areas consisting of both austenite and multi-variants of martensite are scanned by micro-size polychromatic x-rays. Together with the monochromatic energy-scan, structural parameters and deformation gradients are precisely determined, by which the Cofactor Conditions have been examined quantitatively. The continuity condition across a compatible interface is precisely verified for the first time by experiment.

Keywords: Interfaces, Phase Transformation, Microstructure, Laue Microdiffraction

Materials undergoing reversible phase transformations have potential for emerging applications such as medical devices, sensors/actuators, rechargeable batteries, informative storage and energy conversion devices[1–4], and this potential is enhanced by recent discoveries on the origins of hysteresis and reversibility of the martensitic transformation[5–7]. Due to the change of crystal structure, there is a generically stressed transition layer between the austenite and twinned martensite, which has been considered as the leading cause for thermal hysteresis and the failure of reversibility of the transformation. Satisfaction of the Cofactor Conditions (CC)[8,9] implies that such a stressed layer can be eliminated in both single and twinned configurations of austenite and martensite interface microstructure, which has been considered as an effective strategy for lowering the thermal hysteresis, increasing transformational fatigue resistance and enhancing phase reversibility in both copper-based[6] and nickel-titanium[5,7,10,11] based shape memory alloys.

In a typical symmetry-lowering transformation having type I and type II twins consistent with the formal geometry of twinning elements defined by J. W. Christian[12] , CC consists of the two conditions[9]: 1) the middle principle stretch of transformation stretch tensor is 1; 2) the length of a 2-fold axis of austenite is preserved for the forward transformation in the case of type II twin, and for the reverse transformation in the case of type I twin. In the case of compound twins that both twinning plane and shearing direction are rational[13], CC yields different conditions relating to specific twinning parameters (See Chen et al.[9]). A necessary consequence of CC is that, theoretically, there exist infinitely many elastically compatible configurations between austenite and multiple martensite variants without stressed transition layers. The first alloy systematically tuned (by compositional changes) to satisfy the CC conditions for both type I and II twins is $Cu_{25}Au_{30}Zn_{45}$. For more than tens of thousands of thermal cycles, its latent heat does not degrade at all, in sharp contrast to its nearby compositions (i.e. Au_{25} and Au_{27} less closely satisfying CC).

Optical micrographs of $Cu_{25}Au_{30}Zn_{45}$ show a plethora of unusual austenite/martensite interfaces: stripes, curved riverines, zig-zags and laminae[6]. Besides, a great variety of scales has been seen in optical microscope during consecutive transformation cycles. However, direct quantitative verification between these unusual microstructures and those predicted by CC has not been investigated due to three difficulties: 1) owing to a $\sim 2^\circ$ hysteresis in this alloy, the interface moves quickly out of the field-of-view for scanning-based structural characterization probes; 2) the transformation temperature of -40°C is problematic for instruments sensitive to thermal fluctuations; 3) the low symmetry monoclinic martensite with 72 atoms per unit cell with a long modulated c-axis makes the determination of crystal orientation difficult, especially for Electron Diffraction (such as EBSD) methods.

For the above reasons, synchrotron X-ray Laue microdiffraction (μSXRD) becomes the ideal option. This method can characterize the spatial distribution of crystal orientations and deliver the structural parameters using focused polychromatic and monochromatic x-ray beams respectively. In this letter, we use the state-of-art μSXRD facility at beamline 12.3.2 of the Advanced Light Source, Lawrence Berkeley National Lab, to study quantitatively the morphologies of austenite/martensite interfaces in $Cu_{25}Au_{30}Zn_{45}$ undergoing highly reversible martensitic transformation. The X-ray beam with en-

ergy bandpass from 6keV to 22keV is focused down to 1 micron size by a pair of elliptically bent Kirkpatrick-Baez mirrors. In addition to polychromatic beam (i.e. Laue microdiffraction mode), four bounce monochromatic mirrors are inserted to perform energy scans at the same location probed by the polychromatic beam[14], which allows sufficient spatial resolution for determination of twins and solve for the complex lattice with high anisotropic unit cell simultaneously[15]. The 2-dimensional PILATUS 1M array detector with high count rate ($> 2 \times 10^6$ photons/s) is used for fast Laue pattern collection in areas consisting of both phases. Since the μSXRD probe is insensitive to thermal fluctuations, we can design a proper thermal stage that drives the phase transformation at low temperature and controls the evolution of the austenite/martensite interface by an external directional temperature gradient.

The design of thermal stage was implemented using two copper blocks separated by a small gap bridged by a thin slice of sample shown schematically in Figure 1(a). A suitable temperature gradient across the sample is created by passively cooling one copper block with the cryo-nitrogen gas while actively heating the other copper block with an electrical resistance heater. The whole stage is enclosed in a plexiglass box with the top covered by the kapton tape that acts as an window allowing the sample illuminated by x-rays and subsequent transmission of the diffracted x-rays. The stage enclosure is filled with dry nitrogen gas to reduce thermal convection and avoid the formation of frost at low temperature (see Figure 1(b)). The copper blocks are thermally insulated by ceramic standoffs mounted from a kinematic mounting part adapted to the beamline 12.3.2 scanning stage. Two thermocouples, TC_1 and TC_2 in Figure 1(a) record the block temperatures near the gap. TC_2 is also used as feedback for the heater to stabilize the temperature of the hot copper block. The cryo-stream is generated by passing nitrogen gas through a coil in a liquid nitrogen dewar and the cooling power is controlled by a flow meter. The austenite/martensite interface is trapped at the gap and its position controlled by a steep linear temperature gradient established by powering up the electrical heater and running the cryo-stream with a constant rate of 7.86cm^3/s. The actual morphology of the transition varied widely as observed in Song et al.[6], but a typical example is shown in Figure 1(c).

A thin slice $Cu_{25}Au_{30}Zn_{45}$ with dimensions 5mm $\times$ 5mm $\times$ 0.5 mm transforms reversibly between cubic and monoclinic at -40°C with about 2°C thermal hysteresis. The sample was polished at room temperature (in austenite) and mounted to the stage shown in Figure 1(c). After temperatures in TC_1 and TC_2 were stabilized around -65°C and -5°C, respectively, we used a polychromatic $1 \times 1\mu m^2$ beam to start a line scan across the gap and to locate roughly the position where the symmetry of the Laue patterns switches, as shown in Figure 1(a). An area of about 100×100 μm^2 was then targeted for a fine microLaue 2D scan with micron step size.

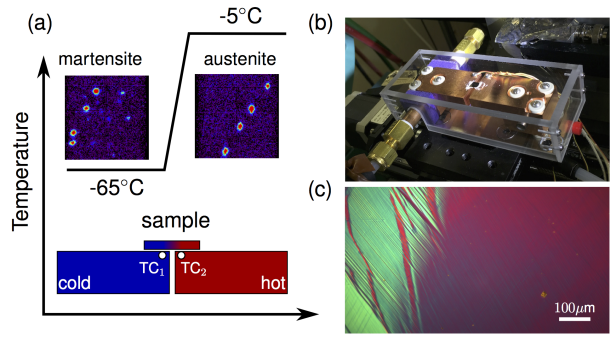

FIG. 1. Experimental setup for in-situ microstructural characterization by μSXRD. (a) Schematic experimental arrangement of sample bridging hot and cold copper blocks (lower). Laue patterns of martensite/austenite at -65°C and -5°C respectively (upper), (b) The temperature gradient stage in plexiglass enclosure with top kapton x-ray window removed. (c) The optical micrograph of the phase-transforming interface of $Cu_{25}Au_{30}Zn_{45}$ polished in austenite (snapshot from the movie in reference Song et al Nature 2013[6]).

To examine the non-reproducibility and diverse interface morphologies of $Cu_{25}Au_{30}Zn_{45}$, we did two microLaue scans for different transformation cycles: LaueScan 1 with step: 4μm $\times$ 10μm and LaueScan 2 with step: 2μm $\times$ 2μm. Holding the conditions constant, the same sample was imaged under the optical microscope for comparison as shown in Figure 2 (b) and (d). The irregular zig-zag and single stripe morphologies are seen in both microtopographs generated by microLaue scans and optical microscopy. Since the images in Figure 2 (a), (b), (c) and (d) are captured in different transformation cycles, the interface configurations among them are not exactly the same.

We use the space group Fm$\bar{3}$m for austenite with 4 Au sites: $4a@(0,0,0)$, 4 Cu sites: $4a@(0,1/2,1/2)$ and 8 Zn sites: $4b@(1/2,1/2,1/2)$, and the space group $P2_1$ for martensite with 18 Au sites: $2a@(3/4,0,z_1+n/9)$, 18 Cu sites: $2a@(1/4,0,z_2+n/9)$ and 36 Zn sites: $2a@(3/4,1/4,z_2+n/9)+2a@(1/4,1/4,z_1+n/9)$ ($n = 1,2,...,9$) to index the Laue pattern and get the orientation matrices for austenite and martensite respectively[14]. The spatial orientations from a microLaue scan consisting of thousands of Laue patterns are analyzed and calculated by the parallel version of the XMAS code on the Carver cluster at National Energy Research Scientific Computing Center (NERSC). Figure 2 (a) and (c) show the microtopographs for LaueScan 1 and 2 respectively, in which various colors represent different spatial orientations whereas the dark blue corresponds to the regions neither indexed by austenite nor martensite. The orientation matrices for each of the regions are listed in Table I. For the indexed (hkl) planes, we precisely measured their interplanar distances by a monochro-

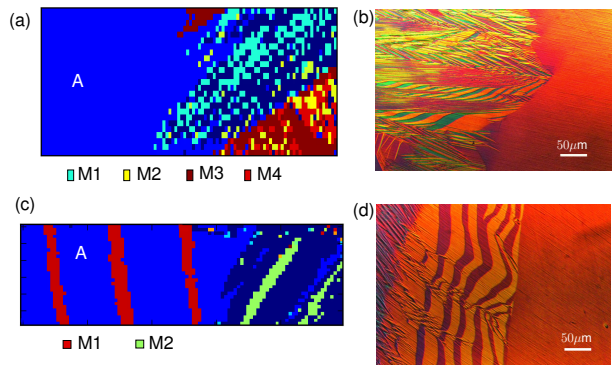

FIG. 2. (a) and (c): Microtopographical configuration in two different transformations from the synchrotron microLaue scan in area of $400 \times 200\mu m^2$ and $200 \times 60\mu m^2$ respectively. The pixel sizes are $4 \times 10\mu m^2$ in (a) and $2 \times 2\mu m^2$ in (c). The austenite is denoted by blue, while each of martensite variants is denoted by different color pixels. The dark blue shows the regions that could not be indexed. (b) and (d): The optical micrographs of the same sample in different transformation cycles.

matic energy scan[16] and refined the lattice parameters to be $a_0 = 6.16061\mathring{A}$ (austenite), and $a = 4.45879\mathring{A}$, $b = 5.76844\mathring{A}$, $c = 40.6984\mathring{A}$, $\beta = 86.79°$ (martensite). Using the *StrucTrans* algorithm[17], the transformation stretch tensor for such a phase transformation can be calculated and the first condition of CC can be quantified precisely, i.e. in LaueScan 1, $\lambda_2(\mathrm{M1}) = 1.00061475$, $\lambda_2(\mathrm{M2}) = 1.00060662$, $\lambda_2(\mathrm{M3}) = 1.00060613$, $\lambda_2(\mathrm{M4}) = 1.00060756$, and in LaueScan 2, $\lambda_2(\mathrm{M1}) = 1.00061044$ and $\lambda_2(\mathrm{M2}) = 1.00061361$.

The second condition of CC requires the examination of length change along certain 2-fold axis of austenite. For the austenite with Fm$\bar{3}$m symmetry, the possible 2-fold axes are three of $< 100 >_\mathrm{a}$ and six of $< 110 >_\mathrm{a}$. They are directly plotted in stereographs in Figure 3 with respective to the Rolling Direction (X), Transverse Direction (Y) and Normal Direction of the stage for LaueScan 1 and 2 respectively. The red dots in all stereographs denote the 2-fold axes of austenite, while the black dots are the $< 901 >_\mathrm{m}$ and $< 991 >_\mathrm{m}$ directions of the corresponding martensite variant. Table I compares the length between the 2-fold axis in austenite and its corresponding direction in martensite. The $< 100 >_\mathrm{a}$ axis undergoes 0.15% average extension, and the $< 110 >_\mathrm{a}$ axis undergoes 0.038% average compression.

From the orientation relationships indicated in Figure 3, we can calculated the deformation gradient $\mathbf{F} = \sum_{i=1}^{3} \mathbf{g}_i \otimes \mathbf{f}^i$ where $\mathbf{f}^i$ are the set of reciprocal lattice vectors of austenite such that the real lattice vectors $\mathbf{f}_i$ correspond to the lattice vectors of martensite $\mathbf{g}_i$ during the phase transformation. Take the M1 region in LaueScan 2 as an example, $\mathbf{f}_1 = \mathbf{O}_\mathrm{a}[010]_\mathrm{a}$, $\mathbf{f}_2 = \mathbf{O}_\mathrm{a}[\bar{1}01]_\mathrm{a}$ and $\mathbf{f}_3 = \mathbf{O}_\mathrm{a}[101]_\mathrm{a}$ correspond to $\mathbf{g}_1 = \frac{1}{9}\mathbf{O}_\mathrm{m1}[\bar{9}01]_\mathrm{m}$, $\mathbf{g}_2 = \frac{1}{9}\mathbf{O}_\mathrm{m1}[9\bar{9}1]_\mathrm{m}$ and $\mathbf{g}_3 = \frac{1}{9}\mathbf{O}_\mathrm{m1}[991]_\mathrm{m}$. Using the orientation matrices $\mathbf{O}_{\mathrm{a,\ m1}}$ listed in Table I, the deformation gradient of M1 region in LaueScan 2 can be calculated as

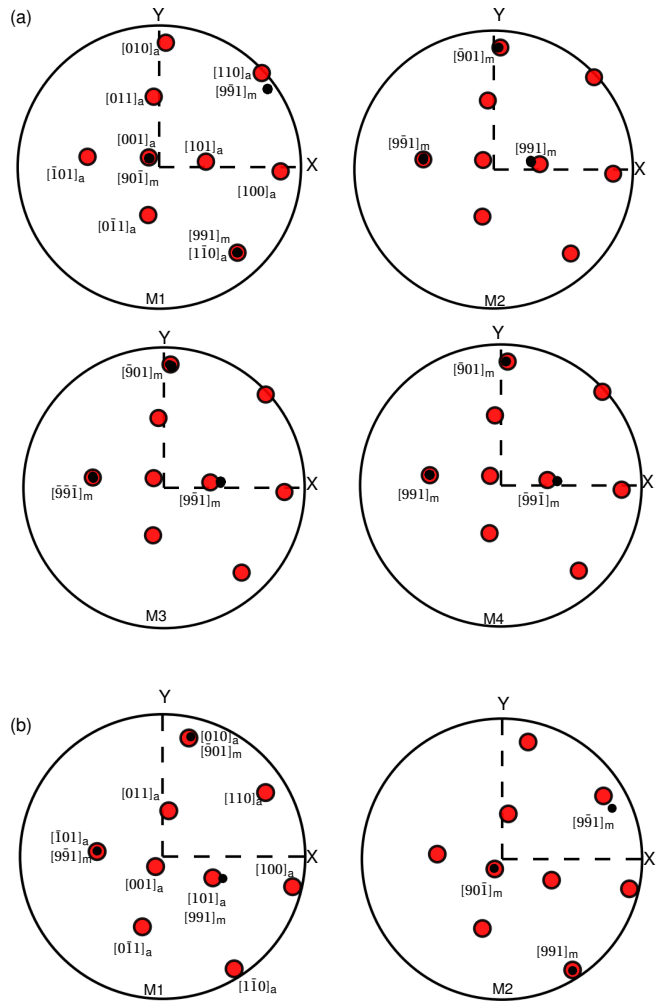

FIG. 3. Stereographic projections of the spatial orientation relationships between austenite 2-fold axes (red dots) and the corresponding martensite lattice vectors (black dots) for (a) LaueScan 1: subregions M1, M2, M3 and M4; (b) LaueScan 2: subregions M1 and M2.

$$\mathbf{F} = \begin{bmatrix} 1.0572 & 0.0049 & -0.0554 \\ 0.0092 & 1.0015 & -0.0119 \\ 0.0627 & 0.0130 & 0.9346 \end{bmatrix}, \qquad (1)$$

which closely satisfies the continuity relation of austenite/martenite interface[18,19] that $\mathbf{F} - \mathbf{I} = \mathbf{b} \otimes \mathbf{m}$ for $\mathbf{b} = (0.652, 0.122, 0.748)$ and the interface normal $\mathbf{m} = (0.0854, 0.0131, -0.0864)$. Figure 4 shows the deformed configuration of the domain containing austenite and the variant of martensite M1 modeled by $\mathbf{F}$ in (1). In 3D, the interface grows into the sample with an angle from the surface, Figure 4 (d) and (e). The projection of the interface can be calculated as $\mathbf{m} - (\mathbf{m} \cdot \mathbf{N}_3)\mathbf{N}_3$, where $\mathbf{N}_3$ is the ND(Normal Direction) of sample surface written in the cubic base of austenite. The angle between

TABLE I. Results of the micro LaueScans. $\mathbf{e}$ is the 2-fold axis of austenite and $\hat{\mathbf{e}} = \mathbf{e}/|\mathbf{e}|$, $X_I = |\mathbf{U}^{-1}\hat{\mathbf{e}}| - 1$ and $X_{II} = |\mathbf{U}\hat{\mathbf{e}}| - 1$.

	region	orientation matrix			$\lvert\mathbf{e}\rvert(\mathring{A})$	$X_I(10^{-3})$	$X_{II}(10^{-3})$
1	A	0.609	0.032	-0.091	6.1606		
		-0.020	0.610	0.082	8.7124		
		0.094	-0.078	0.604	8.7124		
	M1	-0.365	0.065	-2.474	6.17024	1.459	1.563
		0.068	0.57	-0.065	8.70900	8.020	0.371
		0.247	-0.061	-3.231	8.70914	8.044	0.395
	M2	-0.078	0.564	-0.490	6.17018	1.451	1.555
		-0.258	-0.007	3.184	8.70907	8.029	0.381
		0.355	0.12	2.487	8.70900	8.046	0.397
	M3	0.305	0.049	3.100	6.17020	1.453	1.558
		-0.258	-0.007	3.184	8.70904	8.032	0.384
		0.355	0.12	2.487	8.70908	8.033	0.385
	M4	-0.337	-0.050	-2.804	6.17020	1.454	1.558
		-0.317	-0.086	2.634	8.70900	8.037	0.389
		0.074	-0.568	-0.131	8.70902	8.039	0.392
2	A	0.599	0.132	-0.062	6.1606		
		-0.140	0.594	-0.086	8.7124		
		0.041	0.098	0.607	8.7123		
	M1	-0.250	0.023	-3.490	6.17018	1.457	1.561
		0.367	0.081	-2.048	8.70903	8.026	0.378
		0.042	-0.571	-0.433	8.70900	8.039	0.391
	M2	0.278	-0.158	3.118	6.17019	1.461	1.565
		-0.132	-0.548	-0.486	8.70905	8.025	0.376
		0.323	-0.089	-2.570	8.70906	8.033	0.384

the projected interface normal and Rolling Direction (X) is 11.4°, which agrees well with the microLaue measurement shown in Figure 4(a). In Figure 4 (c) we use the deformation gradient $\mathbf{F}$ in Equation (1) to generate a homogenous deformation $\mathbf{Fx}$ for all austenite lattice vectors $\mathbf{x} \cdot \mathbf{m} < 0$, i.e. the red lattice, and leave the rest lattice vectors $\mathbf{x} \cdot \mathbf{m} \geq 0$ undeformed, i.e. the blue lattice. The lattice points between the deformed and undeformed lattices match perfectly without any atomic scale distortions. This is the direct evidence from the μSXRD measurement showing the complete elimination of stressed-transition layer by making lattice parameters satisfy the kinematic conditions of compatibility from macroscopic to atomic scales.

In summary, from the in-situ measurement of the orientation matrices for both austenite and martensite across the interface by the synchrotron x-ray Laue microdiffraction, together with the theoretical calculation of the homogenous deformations, we have verified, directly and quantitatively, that the satisfaction of the conditions of compatibility by lattice parameters results in the stressed-free interface, which ultimately lead to the ultra-low fatigue property of phase transformation in martensitic materials.

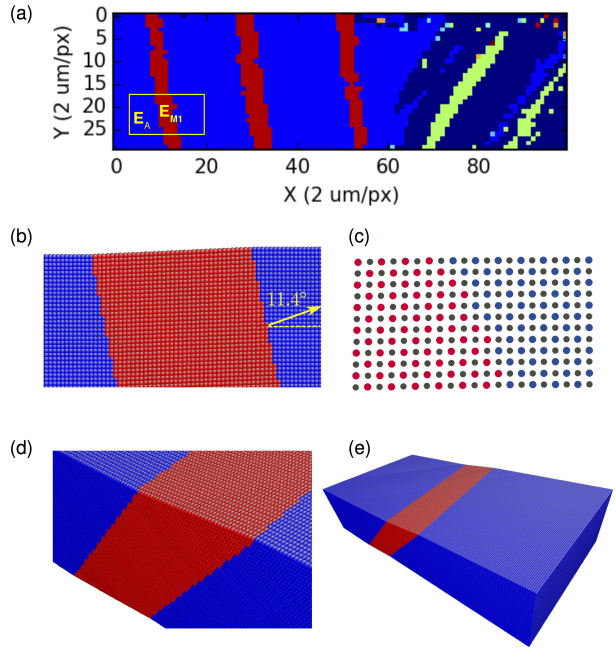

FIG. 4. Macroscopic deformation and lattice distortion of a single variant of martensite calculated from the orientation matrices of $\mathbf{E}_{\mathrm{A}}$ and $\mathbf{E}_{\mathrm{M1}}$: (a) austenite/martensite interface morphology mapped directly from microLaue scan II; (b) homogenous deformation of martensite single variant (red) and the stress-free interface at continuum scale; (c) lattices of austenite and martensite across the interface; (d) and (e) morphology of the interface modeled from the deformation gradient in 3-dimensions.

ACKNOWLEDGMENTS

XC and RDJ acknowledge the financial support of MURI project FA9550-12-1-0458 (administered by AFOSR). This research also benefited from the support of XC's Start-up Fund B002-0172-R9358 (by UGC). The Advanced Light Source is supported by the Director, Office of Science, Office of Basic Energy Sciences, of the U.S. Department of Energy under Contract No. DE-AC02-05CH11231.

[1] N. B. Morgan, Medical shape memory alloy applications—the market and its products, Mater. Sci. Eng., A 378 (1–2) (2004) 16–23. doi:10.1016/j.msea.2003.10.326.

[2] N. Meethong, H.-Y. S. Huang, S. A. Speakman, W. C. Carter, Y.-M. Chiang, Strain accommodation during phase transformations in Olivine-based cathodes as a materials selection criterion for high-power rechargeable batteries, Adv. Funct. Mater. 17 (7) (2007) 1115–1123. doi:10.1002/adfm.200600938.

[3] V. Srivastava, Y. Song, K. Bhatti, R. D. James, The direct conversion of heat to electricity using multiferroic alloys, Adv. Energy Mater. 1 (1) (2011) 97–104. doi:10.1002/aenm.201000048.

[4] J. Liu, T. Gottschall, K. P. Skokov, J. D., M. O. Gutfleisch, Giant magnetocaloric effect driven by structural transitions, Nat. Mater. 11 (7) (2012) 620–626. doi:10.1038/nmat3334.

[5] J. Cui, Y. S. Chu, O. O. Famodu, Y. Furuya, J. Hattrick-Simpers, R. D. James, A. Ludwig, S. Thienhaus, M. Wuttig, Z. Zhang, I. Takeuchi, Combinatorial search of thermoelastic shape-memory alloys with extremely small hysteresis width, Nat. Mater. 5 (4) (2006) 286–290. doi:10.1038/nmat1593.

[6] Y. Song, X. Chen, V. Dabade, T. W. Shield, R. D. James, Enhanced reversibility and unusual microstructure of a phase-transforming material, Nature 502 (7469) (2013) 85–88. doi:10.1038/nature12532.

[7] C. Chluba, W. Ge, R. Lima de Miranda, J. Strobel, L. Kienle, E. Quandt, M. Wuttig, Ultralow-fatigue shape memory alloy films, Science 348 (6238) (2015) 1004.

[8] R. D. James, Z. Zhang, A way to search for multiferroic materials with "unlikely" combinations of physical properties, in: A. Planes, L. Mañosa, A. Saxena (Eds.), Magnetism and structure in functional materials, Springer Berlin Heidelberg, 2005, pp. 159–175.

[9] X. Chen, V. Srivastava, V. Dabade, R. D. James, Study of the *cofactor conditions*: Conditions of supercompatibility between phases, J. Mech. Phys. Solids 61 (12) (2013) 2566–2587. doi:10.1016/j.jmps.2013.08.004.

[10] Z. Zhang, R. D. James, S. Müller, Energy barriers and hysteresis in martensitic phase transformations, Acta Mater. 57 (15) (2009) 4332–4352. doi:10.1016/j.actamat.2009.05.034.

[11] R. Zarnetta, R. Takahashi, M. L. Young, A. Savan, Y. Furuya, S. Thienhaus, B. Maaß, M. Rahim, J. Frenzel, H. Brunken, Y. S. Chu, V. Srivastava, R. D. James, I. Takeuchi, G. Eggeler, A. Ludwig, Identification of quaternary shape memory alloys with near-zero thermal hysteresis and unprecedented functional stability, Adv. Funct. Mater. 20 (12) (2010) 1917–1923. doi:10.1002/adfm.200902336.

[12] J. W. Christian, The Theory of Transformations in Metals and Alloys (Part I + II), Pergamon, 2002.

[13] K. Bhattacharya, Microstructure of martensite: why it forms and how it gives rise to the shape-memory effect, Oxford series on materials modeling, Oxford University Press, 2003.

[14] N. Tamura, XMAS: a versatile tool for analyzing synchrotron x-ray microdiffraction data, Imperial College Press (London), 2014.

[15] K. Moffat, D. Szebenyi, D. Bilderback, X-ray laue diffraction from protein crystals, Science 223 (4643) (1984) 1423.

[16] M. Kunz, N. Tamura, K. Chen, A. A. MacDowell, R. Celestre, M. Church, S. Fakra, E. Domning, J. Glossinger, J. Kirschman, G. Morrison, D. Plate, B. Smith, T. Warwick, V. Yashchuk, H. Padmore, E. Ustundag, A dedicated superbend x-ray microdiffraction beamline for materials-, geo- and environmental sciences at the Advanced Light Source, Review of Scientific Instruments 80 (3) (2009) 035108.

[17] X. Chen, Y. Song, N. Tamura, R. D. James, Determination of the stretch tensor for structural transformations, arXiv:1501.05064.

[18] M. S. Wechsler, D. S. Lieberman, T. A. Read, On the theory of the formation of martensite, Trans. AIME (1953) 1504.

[19] J. M. Ball, R. D. James, Fine phase mixtures as minimizers of energy, Arch. Ration. Mech. Anal. 100 (1) (1987) 13–52. doi:10.1007/BF00281246.